A cryogenic linear ion trap beamline for providing keV ion bunches

Menk, S.; Bertier, P.; Enomoto, Y.; Masunaga, T.; Majima, T.; Nakano, Y.; Azuma, T.

Review of Scientific Instruments

A cryogenic linear ion trap beamline for providing keV ion bunches

Cite as: Rev. Sci. Instrum. **89**, 113110 (2018); https://doi.org/10.1063/1.5051044
Submitted: 05 August 2018 . Accepted: 23 October 2018 . Published Online: 14 November 2018

S. Menk, P. Bertier, Y. Enomoto, T. Masunaga, T. Majima, Y. Nakano, and T. Azuma

REVIEW OF SCIENTIFIC INSTRUMENTS **89**, 113110 (2018)

A cryogenic linear ion trap beamline for providing keV ion bunches

S. Menk,[1,2,3,a)] P. Bertier,[1,4] Y. Enomoto,[1,5] T. Masunaga,[1] T. Majima,[2,6] Y. Nakano,[1,3] and T. Azuma[1,2]

[1]*AMO Physics Laboratory, RIKEN, Wako, Saitama 351-0198, Japan*
[2]*Department of Physics, Tokyo Metropolitan University, Hachioji, Tokyo 192-0397, Japan*
[3]*Department of Physics, Rikkyo University, Tokyo 171-8501, Japan*
[4]*Université de Lyon, F-69003 Lyon; Université Lyon 1, Villeurbanne; and CNRS/IN2P3, UMR5822, Institut de Physique Nucléaire de Lyon, F-69622 Villeurbanne, France*
[5]*Accelerator Laboratory, KEK, Tsukuba, Ibaraki 305-0801, Japan*
[6]*Department of Nuclear Engineering, Kyoto University, Kyoto 615-8540, Japan*

(Received 5 August 2018; accepted 23 October 2018; published online 14 November 2018)

A new cryogenic linear ion trap beamline has been constructed and commissioned, which serves to inject cold molecular and cluster ions into the RIKEN cryogenic electrostatic ring (RICE). Ions are created with an electrospray ion source, and a quadrupole mass filter is used for mass-selection prior to trap injection. The radio frequency octupole ion trap can be continuously loaded with ions and features a fast ion extraction mode to create short ion bunches with tens of μs duration. We report here on the simulations and development of the ion trap beamline and validate performance with the moderately heavy molecular cation methylene blue. Characterization of the novel trap design with additional wedge-shaped electrodes was carried out, which includes the determination of the temporal and spatial shape of the ion bunch and the total number of ions after extraction. Finally, these ion bunches are synchronized with the switching of a pulsed high-voltage acceleration device downstream of the trap, where the ions obtain a kinetic energy of up to 20 keV. The preparation and control of the keV ion beam are demonstrated for the ion injection into RICE. https://doi.org/10.1063/1.5051044

I. INTRODUCTION

Radio frequency (RF) ion traps[1] developed decades ago can keep low-velocity ions in a confined space in gas-phase. Ion-neutral collisions with a buffer gas reduce the ions' kinetic energy and eventually thermalize the internal degrees of freedom of molecular ions. In cryogenic traps, the gas is cooled at first by contact with the cold surroundings, and finally ions and gas approach thermal equilibrium. Low and well-defined internal excitation of the molecular ions will benefit spectroscopic measurements as it simplifies the obtained spectra and improves comparability to theoretical models. Commonly, laser spectroscopy and ion-neutral reactions are performed inside the trap, while the ions are detected after their extraction from the trap. Quadrupole mass filters before and behind the trap are used to analyze the initial and final states of the reaction,[2] or the products are identified by a time-of-flight measurement.[3] Disadvantages are the loss of precise temporal information of the reaction due to the product extraction as well as often continuous energy exchange with the buffer gas during the reaction in the trap. Fast spectroscopic measurements might be accessible via trap *in situ* detection of the fluorescence light;[4,5] however, this method exhibits a low efficiency and requires luminescence emission from the molecule of interest.

On the other hand, storing ions as a fast moving beam under ultra-high vacuum makes precise temporal observation of reactions in the microsecond range possible and for extended time (microseconds to minutes) under isolated conditions. Since ion storage rings were introduced, experiments benefited from the repetitive use of the stored isolated ions and long observation times. Electrostatic ion storage rings[6–8] and electrostatic ion beam traps[9] are intended to study fundamental properties of large molecules; however, one of their limitations is in preparing cold molecular ions. While the cold environment of recently developed cryogenic storage rings[10–12] and traps[13,14] keeps the ions from reheating due to blackbody radiation from the surroundings, the radiative cooling itself of vibrational and rotational excitation is often limited by the low infrared activity and slow relaxation times. For instance, the radiative lifetime of the lowest rotational state in small diatomic ions like HD^+ was calculated to be as long as 140 s.[15] Recent experiments in cryogenic storage rings on OH^- found radiative lifetimes for $J = 1$ of 193 s[16] and 183 s,[17] respectively. The latter group also succeeded to effectively cool an ensemble of stored OH^- ions by photo-detachment of the non-ground state levels.[18] Except for these special cases, efficient internal cooling mechanisms prior to ion injection need to be employed such as low velocity collisions with a cold gas.

II. CONCEPT AND DESIGN

We introduce an ion preparation beamline with a cryogenic RF ion trap intended to accumulate and cool molecular ions to their rovibrational ground states and subsequently inject them into our new storage ring RICE (RIKEN cryogenic

a)sebastian.menk@riken.jp

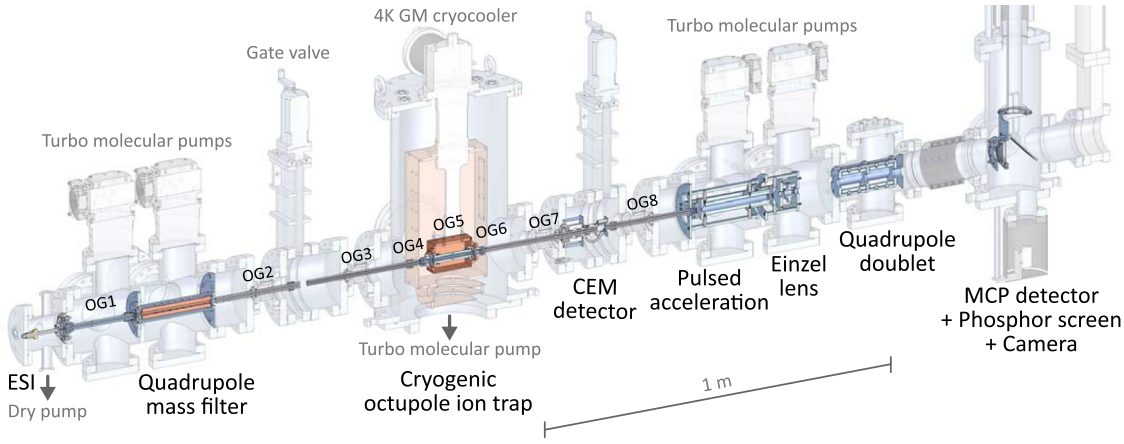

FIG. 1. Schematic view of the entire cryogenic trap beamline (OG: octupole guides).

electrostatic ring)[12] at RIKEN, Wako, Japan. Other cryogenic storage ring groups are also working on similar ion injection systems.[19] Ion production for the present beamline at RIKEN is performed via electrospray ionization (ESI) but can be replaced by other low-energy ion sources. Efficient ion transportation is accomplished by RF octupoles and mass-selection with a quadrupole mass filter. Essential aspects are the fast extraction of ions from the trap and the pulsed acceleration to kinetic energies of up to 20 keV to meet the operation requirements of RICE. All parts of the setup (see Fig. 1) with their characteristic features will be introduced in detail in Secs. II A–II F.

A. Electrospray ionization source

The method of the electrospray ionization was developed in the 1980s[20,21] to bring large molecules from liquid into gas-phase and is nowadays a widely distributed tool in mass analysis of large biomolecular species such as proteins.[22] One of the characteristic features is the so-called soft ionization, which predominantly retains the intact molecules during the evaporation process. This is achieved by ionizing the molecule of interest inside a droplet of the solvent which protects it from collisional dissociation. After evaporation of the solvent, the ionized bare molecule remains.

In general, the ionization is performed with a static high voltage of about 2-5 kV between a liquid-filled needle and a capillary, through which the ions are introduced into the vacuum system. Positively and negatively charged molecules on the tip of the needle are separated and are accelerated toward the capillary according to the polarity of the voltage. In this gap, the evaporation of the solvent takes place and is often supported by a surrounding warm nitrogen flow. Collisions inside the capillary also support this evaporation, which can be promoted by heating.

We have developed a home-built ESI source (Fig. 2) which uses a heated capillary (Thermo Fisher) but without the warm nitrogen gas flow (the initial design of a prototype beamline was reported elsewhere[23]). The needles are purchased from Hamilton (e.g., 26 gauge, Small Hub RN NDL, point style AS), and a glass coupler (Hamilton) is used for isolation when applying high-voltage to the needle. The liquid flow through the needle is controlled by using a syringe pump (YMC YSP-101) between 10 μl/h and 100 μl/h. Ions leaving the capillary on the vacuum side are focused by using a cylindrical lens before they pass through a conical skimmer (1 mm diameter aperture) into an octupole ion guide.

B. Radio frequency ion guides and quadrupole mass filter

Low kinetic energy ions from the ESI of ≤30 eV are transported by eight separate RF octupole ion guides (OG1-OG8), where OG5 serves as an ion trap with 110 mm length (see Fig. 1). The electrodes are stainless-steel rods with a diameter of 3 mm and an inner diameter separation of 9 mm. OG1 is

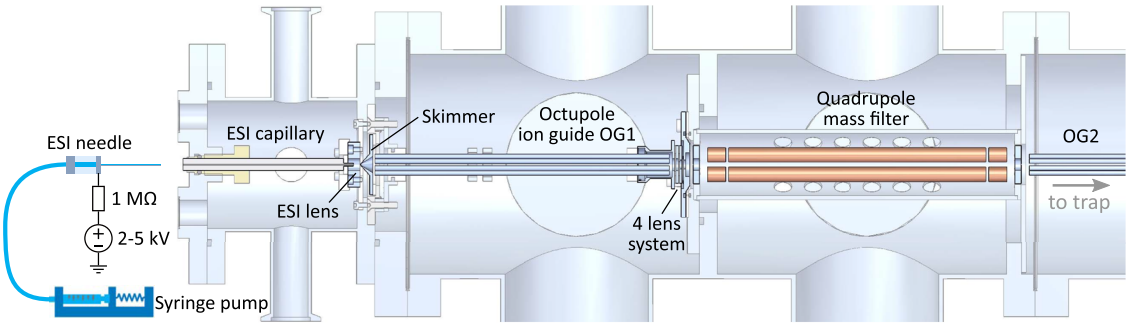

FIG. 2. Electrospray ionization (ESI) source with octupole guide OG1 and a quadrupole mass filter.

197 mm long and connects the ESI to the quadrupole mass filter. The other octupoles are symmetrically arranged with respect to the ion trap with lengths $L_{OG2} = L_{OG8} = 246$ mm, $L_{OG3} = L_{OG7} = 326$ mm, and $L_{OG4} = L_{OG6} = 33$ mm (entrance and exit of the trap). Four home-built RF oscillators (based on the work of Jones and Anderson[24]) have been optimized to a frequency of ~1.2 MHz and are used to apply the RF voltage of typically 200 V and individual DC voltages to each octupole.

For the guiding of light ions ($\lesssim$100 amu) through the octupoles, a higher RF is required and another RF system was designed (Fig. 3) which uses a 5 MHz sinusoidal wave from a function generator (Keithley 3390) and an RF power amplifier (R&K-ALM000110-2840FR-R). A standing wave ratio and power meter (Diamond Antenna SX200) is used to measure the transmitted and reflected power and to protect the amplifier from reflections (not shown in Fig. 3). The RF signal is then connected to four coupling circuits for transforming the voltage, for impedance matching, and for applying a DC component to the RF voltage. This is accomplished with a toroid ferrite core (type T200-2) with $N_1 = 2$ and $N_2 = 18$ windings on the input and output, respectively.

Octupoles are combined in parallel to obtain similar capacitances on each ferrite core and to reduce the capacitance from cables by choosing octupoles with close proximity as follows: OG1, OG2/OG3, OG4/OG5/OG6 as well as OG7/OG8. Each of the four coupling circuits has a total capacitance of approximately 200 pF; 120 pF were added in parallel to OG1 to accomplish this. The resonance frequency of the octupole circuit is defined by the inductance on the output side of the core ($N_2 = 18$, $L_2 \approx 0.012 \cdot N_2^2 \approx 3.9\mu$H), and the capacitances of the octupoles, the cables C_{cable}, and the variable capacitance C_{tune} (maximum 100 pF). The latter capacitance is sufficient to tune all resonance frequencies to 5 MHz (total capacitance ~250 pF), and all octupoles are operated by only a single function generator and amplifier. RF amplitudes of up to 400 V can be achieved, while the DC voltages are applied to each octupole individually.

To mass-select the ions from the ESI prior to the trap, a Tri-filter Quadrupole Mass Filter (Extrel) with a total length of 200 mm and 9.5 mm diameter rods is used. Two power supplies

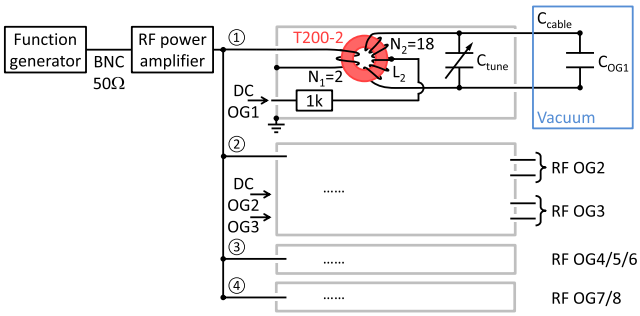

FIG. 3. Schematic circuit diagram of the RF concept for 5 MHz. After RF generation and amplification, four circuits are used to combine octupoles (OG1, OG2/OG3, OG4/OG5/OG6, OG7/OG8), transform the voltage, match impedance, and apply a DC voltage to the RF. Circuit for OG1 is shown in detail (except for missing 120 pF in parallel to C_{tune}). The other circuits are equivalent with multiple secondary windings on the same ferrite core (see text for more details).

(Extrel 150-QC) are utilized alternatively with resonators at 440 kHz (mass range 20-16 000 amu) and 1.2 MHz (mass range 2-1000 amu), respectively.

C. Cryogenic ion trap

The cryogenic ion trap consists of one long (OG5) and two short octupole guides (OG4/OG6) with two cylindrical end-caps (EC1/EC2) in between, which are used for the longitudinal ion confinement [see Figs. 4 and 5(a)]. The octupole rods are mounted with AlN ceramic holders on the copper inner radiation shield, which is connected to the second stage of a Gifford-McMahon (GM) type cryocooler (Sumitomo compressor F-50Lw, cold head RDK-408D2), while the outer radiation shield is cooled by the first stage. Three silicon diode sensors are used to monitor the temperatures at specific locations on the upper and lower parts of the inner shield as well as on the outer shield. Final temperatures measured at these positions were 5.7 K, 6.2 K, and 26 K, respectively, and the cooling process from room temperature takes about 2 h. Two 25 W ceramic heaters are installed on the top of the inner shield and can be used to vary the trap temperature with a precision of less than 1 K. Helium gas is injected into the inner trap shield using a copper pipe, which is thermally connected to the outer shield to precool the helium gas. A pulsed valve (Parker) is used to introduce the helium and is typically operated with a rate of 10 Hz (<200 μs valve opening). This allows inhibition of helium injection before the ions are extracted from the trap and thus reduces reheating by heavy ion-helium collisions.

Figure 5(b) illustrates the trap potential in the longitudinal direction along the trap axis for ion injection, trapping, and extraction. For the continuous ion injection into the trap, the potential on the entrance end-cap is low enough to allow ion injection, while the exit potential reflects the ions. The former potential is optimized taking into account the kinetic energy of the ions such that ions cannot leave the trap after they have lost

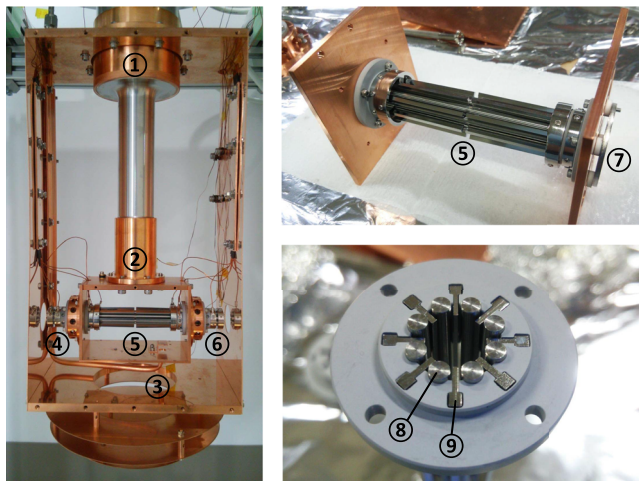

FIG. 4. Left side: Photos of the octupole trap with the cold head of the GM cryocooler's first stage (1) connected to the outer radiation shield and the second stage (2) to the inner. Helium injection tube (3) connected to the inner trap shield and octupole guides OG4, OG5 (trap), and OG6 with numbers (4)-(6), respectively. Right side: Detailed view of the trap end-cap ring-electrode (7) and arrangement of the trap rods (8) and fin-shaped electrodes (9).

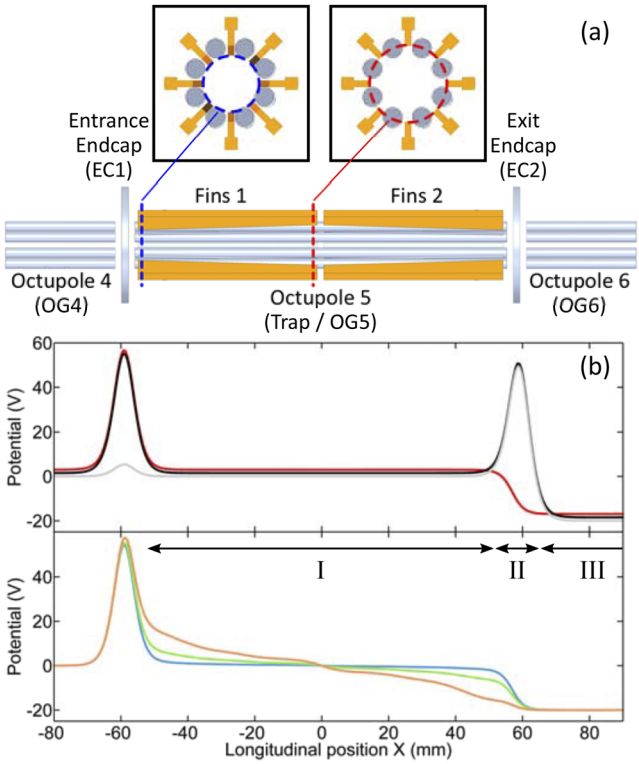

FIG. 5. (a) Side view of the trap with fin-electrodes. The fins' radial distance to the trap axis increases linearly from the trap entrance (4.5 mm) toward the trap center (6 mm), as seen in the two cross section views (blue and red circles). (b) Simulated trap potential on the trap axis: Injection (gray), trapping (black), and ion extraction without fins (red). Potentials are slightly vertically shifted for visibility. Ion extraction potential with fin-voltages of ±5 V, ±20 V, ±50 V are shown in blue, green, and orange, respectively. The first and second acceleration regions are marked by I and II, and the beginning of the drift region with III (see text for details).

a part of their energy by collisions with helium. The helium density in the trap is adjusted for sufficient collisional cooling. After a trapping period, the potential at the exit end-cap is lowered for the ion extraction. Here, the flat longitudinal trap potential, which is suitable for trapping and cooling of the ions, poses a problem in extracting the ions as a short bunch. There have been several methods to support the fast extraction by modifying the trap design,[25–28] and in this work, we developed a new concept.

To enable fast ion extraction in the present trap, two sets of eight additional wedge-shaped electrodes, hereafter called "Fins", have been placed between the octupole rods of the trap [Fig. 5(a)]. This is one of the important features of the present trap, as these fin-electrodes create a longitudinal gradient field when a voltage is applied. Both sets are mirror-symmetrically arranged with respect to the trap center, where the shorter side of the wedges points toward this center [see Fig. 5(a)]. Due to this arrangement, the potentials at the trap entrance and exit experience a stronger influence from the fin-voltages, which leads to the longitudinal gradient. Typically, a positive voltage is applied to the entrance-fins and a negative to the exit-fins with respect to the DC voltage on the trap octupole. During ion injection and trapping, the potential remains flat, which provides the highest capacity for ion trapping (compared to other implementations with a permanent potential minimum inside the trap[25]). Both sets of fins as well as the two end-caps are connected to individual fast voltage switches, which allow for rapid changes to the applied voltages exclusively during the ion extraction phase (time constant of $\tau \approx 50$ ns).

In other implementations of bunched ion trap extraction, segmented rods are used.[25] All of them require different voltages to be supplied, and additionally higher voltages are also needed for ring electrodes around the rods.[26] The advantage of two sets of fins, compared to other reported designs with only a single set of these electrodes,[27–29] is the mirror symmetric arrangement with respect to the trap center (Fig. 5). The potential around the trap center is thus not influenced by the fins as their thinner sides do not reach radially between the rods. By contrast, the longitudinal trapping potential of the end-caps prevents ions from being trapped near the locations where the thicker sides of the fins extend into the inside of the trap. Furthermore, because the gradient potential during extraction is centered around the trap offset (DC voltage on OG5), the ion's mean kinetic energy is solely given by the potential difference between this offset and that of the next octupole OG6. Finally, the two sets of fins offer more flexibility in controlling the shape of the potential, which is important for the extraction and focusing method explained in more detail in the simulation section.

D. Pulsed high-voltage acceleration

For the ion transport and injection into RICE, the cold ions from the trap need to be accelerated to a kinetic energy of up to 20 keV. We employed an ion acceleration device which operates with a pulsed high-voltage and accelerates short (tens of microseconds) ion bunches. The pulsed acceleration device is installed inside the vacuum chamber, and high-voltage is only used in a short section of the whole beamline. This pulsed scheme fits well to the RICE ion injection, as ions need to be always bunched. By contrast, ion sources are commonly installed on high-voltage platforms and the acceleration occurs when ions leave this high potential. The drawback of this arrangement is the need for a large high-voltage cage, isolated mounting as well as no direct access to the setup during operation.

The acceleration device consists of a 200 mm long stainless-steel tube placed behind the last octupole guide OG8 (more details are given later in Fig. 10). This tube is connected to a 20 kV high-voltage switch (based on a Behlke HTS 241-20-GSM) and is quickly switched (time constant of $\tau \approx 100$ ns) between a low negative potential and the positive high-voltage. Ion bunches injected into the tube are lifted to high potential and accelerated while leaving the tube on the opposite side. Lenses at the entrance as well as a conical high-voltage lens at tube potential and an einzel lens at the exit are used to focus the ion beam (see Fig. 10).

E. Vacuum system

The vacuum system is separated into six differential pumping sections. The first is the ESI vacuum chamber which is pumped by using a dry vacuum pump (Edwards iGX600N) and reaches an operation pressure of about 50 Pa. As shown in Fig. 2, a skimmer (diameter 1 mm) separates the source from

the next chamber containing OG1 and the quadrupole mass filter. The latter two elements are divided by a four-lens system (8 mm inner diameters), and each section is pumped with a turbomolecular pump (Osaka TG220F) to a pressure of the order of 10^{-1} Pa and 10^{-4} Pa, respectively. Differential pumping of the trap chamber is realized by the two long octupole guides OG2 and OG3. A turbomolecular pump (Osaka TG1100F) is used to pump the trap chamber, and a pressure of $\sim 10^{-6}$ Pa is obtained. The chamber containing the acceleration tube and einzel lens is equipped with two turbomolecular pumps (Osaka TG220F) and reaches a similar pressure to that in the trap chamber. During helium injection into the trap, the pressures in the trap and acceleration tube chambers increase to 10^{-2} Pa and 10^{-4} Pa, respectively.

Additionally, the vacuum chambers are movable due to being mounted on a multi-rail system and connected with four bellows (locations of the labels for OG2, OG3, OG7, and OG8 in Fig. 1). This design allows the chambers to move relative to each other while maintaining vacuum and alignment. Three locations in the beamline take advantage of this system, which are the gate valve between OG2 and OG3, the ion trap, and the ion detector. For maintenance of the ion source while keeping the trap under vacuum and cryogenic conditions, the multi-rail system is employed to provide sufficient separation between OG2 and OG3 to allow for closure of the gate valve (Fig. 1). Second, in order to remove the ion trap for maintenance purposes, the octupoles OG3 and OG7 need to be retracted from the outer radiation shield of the trap. The third location will be introduced in Sec. II F.

F. Ion detection systems

Several ion detection methods are employed depending on the purpose. Octupole ion guides can be disconnected from the RF source and used as a Faraday cup to collect the ion charges by connecting it to a picoammeter (Keithley 6485). An additional small negative offset voltage is optionally used to improve the charge collection (e.g., by connecting an 18 V battery in series). Typically a current of 10-100 pA was thus measured on OG1 for ions from the ESI source. The transmission to OG7 was estimated to be about 50%. For precise timing information of bunched ions, a current preamplifier (ITHACO model 1211) is connected to the octupole to determine the absolute number of ions in a bunch after trap extraction or when a pulsed ion source is used.

Additionally, a channel electron multiplier (CEM, DeTech 402AH) with a high-voltage converter plate was placed behind octupole OG7 to measure the ion count rate (see Fig. 1 for the location). Figure 6 illustrates the principle of the CEM detector and the two operation modes of ion-guiding and ion-detection. For the normal ion-guiding operation, octupoles OG7 and OG8 are as close as a few millimeters apart, as shown in Fig. 6(a), while for the detection mode with the CEM, the gap is increased to ~20 mm [Fig. 6(b)]. Ions in the gap between these octupoles are accelerated to the converter plate at −4 kV, the produced secondary electrons travel to the entrance of the opposing CEM kept at about −2 kV, and the amplified electron signal is collected at the end of the CEM. For this purpose, the CEM and acceleration tube chambers are connected

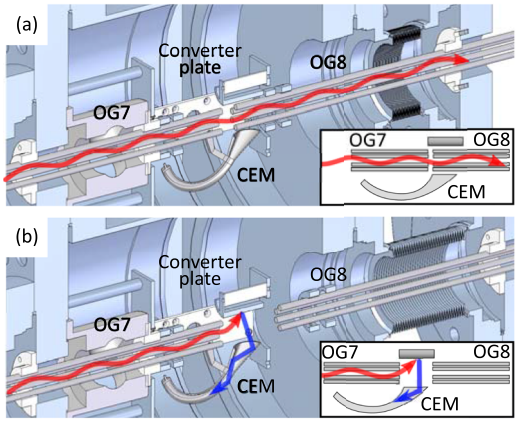

FIG. 6. CEM detector integrated in octupole guides: (a) Ion-guiding mode with a small gap between OG7 and OG8 and (b) ion detection mode with a large gap between OG7 and OG8. The ion path is shown in red; the electron path is shown in blue.

with bellows and mounted on rails as introduced beforehand. With this method, the two modes of efficient ion-guiding and ion-detection can be switched easily.

Ions from the acceleration tube with keV energies are detected with a micro-channel plate (MCP, Photonis) detector in a chevron configuration with a phosphor screen (both 40 mm diameter). It is mounted on a movable support about ~700 mm downstream of the acceleration region. A quadrupole doublet in between is utilized to optimize the ion bunch shape for further ion transport to the injection beamline. The 2D image on the phosphor screen is detected by using a triggerable camera through a flat mirror and a vacuum window. Thus, ion bunch timing and shape can be monitored simultaneously.

III. ION TRAJECTORY SIMULATIONS

For the efficient injection of ions into RICE, bunched ion extraction from the trap and pulsed high-voltage acceleration need to be combined so that the length of the ion bunches is as short as the acceleration tube. The additional fin-electrodes of the trap already introduced in Sec. II C are used to create the longitudinal gradient potential for extraction.

It is noted that the ions are actually not extracted as a short bunch from the trap but rather focused in time to a specific position behind the trap. To satisfy this condition, a method from Wiley and McLaren[30] is used. They presented a two-step ion acceleration which can partly compensate the initial ion distribution in a time-of-flight mass spectrometer. The basic idea is to introduce a velocity spread in the first stage, which gives a higher velocity to ions with a larger distance to the detector and vice versa. The second acceleration stage is adjusted in a way that all ions with the same mass will reach the detector at the same time regardless of their initial position.

We adapted this idea not to mass-separate ions but rather create short ion bunches of the same mass from a wide ion distribution in the longitudinal direction in the linear ion trap. The configuration is separated into an acceleration region inside the trap [region I in Fig. 5(b)], an acceleration region at the trap exit (region II), and a drift region in the following octupole ion guides OG6-OG8 (region III). The short second

acceleration region II between the trap exit and OG6 only introduces minor energy dispersion and mainly acts as an adjustment for the final velocity of the ions.

A. Ion trajectory simulations of the ion trap

The trap extraction of methylene blue cations MB^+(mass 284 amu) was simulated with SIMION[31] using a RF frequency and voltage of 1.2 MHz and 200 V, respectively. Simulated trajectories of ions from the trap to the entrance of the acceleration tube are shown in Fig. 7 for three different fin-voltages as a function of the time after trap extraction. In the case of (a), the fin-voltage of ±50 V (+50 V on entrance-fins and −50 V on exit-fins) is too high leading to a focus point of the trajectories before the target position. (b) shows appropriate focusing with ±20 V and a short bunch, and (c) with ±1 V uses a too low voltage.

Figure 8 shows the simulation results of the ion's arrival time distribution, namely, bunch shape, after trap extraction at the position of the CEM detector, which is used to monitor the ion bunch experimentally and is located behind octupole OG7 (distance from the trap center to the end of OG7 is 426 mm). Note that this position is now different compared to Fig. 7, to make the simulation results better comparable to the measurements with the CEM. For each setting, 10 000 ions were randomly placed in the trap and the extraction was performed with fin-voltages of ±20 V, ±5 V, ±1 V, and 0 V, respectively. In the case of (a), no initial kinetic energy (*KE*) was assumed and isotropically distributed kinetic energies in the other cases with 0.05 eV (b), 0.1 eV (c), 0.5 eV (d), and 1 eV (e). The ion trajectories were simulated individually, and thus no Coulomb repulsion between ions was considered. For ions at room temperature, a kinetic energy of about 40 meV is expected (assuming $KE = 3/2k_BT$).

Without the initial kinetic energy of the ions in (a) and a fin-voltage of 0 V, no ions reach the position of the CEM in the plotted time, while increasing the kinetic energy makes a bunch visible. With higher fin-voltages, the bunch length decreases

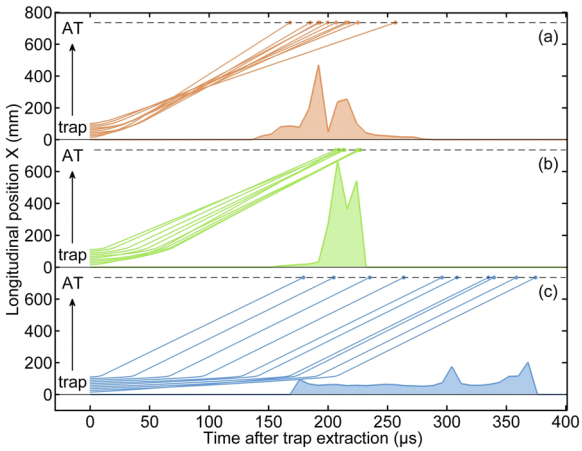

FIG. 7. Simulated ion trajectories from different positions along the longitudinal trap axis to the acceleration tube entrance (AT) versus time after trap extraction using fin-voltages of ±50 V (a), ±20 V (b), and ±1 V (c). The histogram of the arrival times is also shown using a larger number of simulated ions than displayed trajectories. The initial kinetic energy was set to 0 eV; the trap (OG5) was at 0 V; and OG6, OG7, and OG8 were at −20 V.

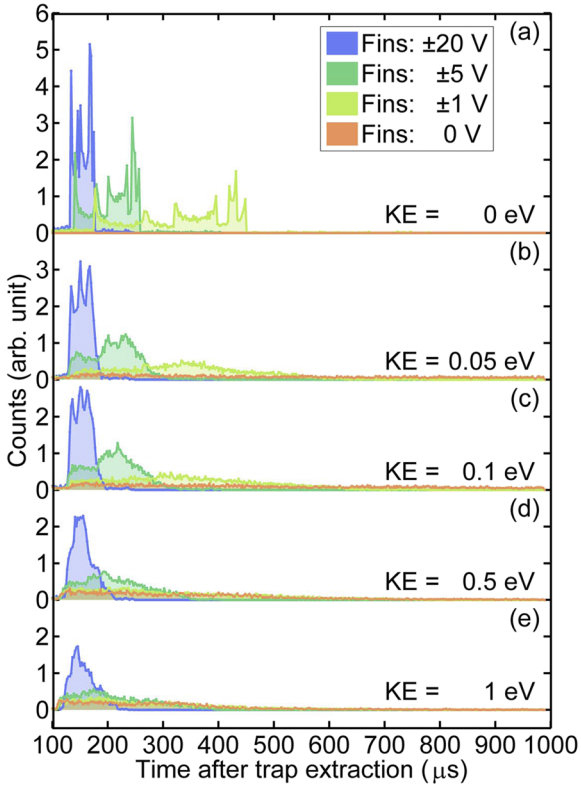

FIG. 8. Histograms of simulated ion arrival times (bunch shapes) at the location of the CEM detector after trap extraction with different fin-voltages of ±20 V, ±5 V, ±1 V, and 0 V. 10 000 ions were randomly created in the trap volume (using a cylinder with 1 mm radius and 100 mm length), trapped for 10 μ and extracted. Isotropically initial kinetic energies (*KE*) of the ions were (a) 0 eV, (b) 0.05 eV, (c) 0.1 eV, (d) 0.5 eV, and (e) 1 eV.

and is about 50 μs for fins of ±20 V in cases (a) to (c). We will compare these simulated bunch shapes with the experimental results to obtain a rough estimate of the kinetic energy of the ions in the trap. The sharp distinct features in (a) are simulation artifacts and arise because ions without kinetic energy are more sensitive to the shape of the extraction potential. They rapidly disappear under more realistic conditions with a small kinetic energy as in (b).

During the trap extraction, a kinetic energy spread in the ion bunch will be introduced which is easily estimated from the potential in Fig. 5. For instance, a full width at half maximum of about ±6 eV is expected from fin-voltages of ±20 V, while the mean kinetic energy of 20 eV originates from the potential offset between the trap and OG6/7 of −20 V. Considering that the ions are accelerated to at least 10 keV, the energy resolution results to be better than three orders of magnitude (i.e., kinematic compression). In comparison, the energy acceptance $\Delta E/E$ of the RICE ring was measured to be of the order of 10^{-3}. The bunch length is adjustable depending on the circulation period of the ions in the RICE, which depends on the mass of the ions (for instance, 36 μs for MB^+ at 10 keV). If necessary, the energy spread can be reduced at the expense of the bunch length.

B. Simulation on the space-charge limit of the trap

In an independent crude simulation (using MATLAB[32]), the maximum number of ions that can be stored in the trap

limited by Coulomb repulsion between the ions (space-charge) was evaluated. As reported previously,[33] high charge densities in an octupole trap will push the ions toward the octupole rods. The counteracting forces in the radial direction from the octupole field and the ion's Coulomb repulsion compensate each other in such a way that an enhanced ion density is acquired for a larger radial position. By contrast, a flat distribution would be obtained for a quadrupole potential as this increases more steeply than that of an octupole. The space-charge limit of the trap is reached when this average ion radius expands too close to the position of the trap rods and ions are lost due to collisions with them.

In our simulation, we adapted an octupole potential in the radial direction and used the trapping potential from Fig. 5 as a longitudinal confinement. Initially, singly charged ions were randomly created in the trap within a cylindrical volume with 3 mm radius and 100 mm length. Their trajectory was followed for a total time-of-flight of 10 μs using time steps of 10 ns.

To consider the ions' interaction with both the trap potential and their instantaneous Coulomb repulsion, it is desirable to deal with a large number of ions simultaneously. To make the simulation more tractable, the movement of 1000 ions was simulated and the location of these ions in each time step was used to generate the space-charge density in the trap. To imitate a higher space-charge than the number of simulated ions, each ion was exclusively for this purpose assumed to be multiply charged.

These simulations were performed under the conditions of different total charges up to $10^{10}e$. The case assuming no charge repulsion was also tested for comparison. Smaller time steps of 1 ns, an increased total time-of-flight of 100 μs as well as the cases of 100 and 10 000 ions (keeping the total charge of the stored ions constant) were also tested for several simulations. These confirm the stability and robustness of the simulation parameters and provide reasonably similar results.

For low space-charge, e.g., below 10^6e in the simulation, no effect from the Coulomb repulsion was observed when compared to the simulation without any ion repulsion. For higher space-charge of 10^7e and 10^8e, a clearly increased ion radius is obtained. Figure 9 shows the critical cases of 10^8e (a) and 10^9e (b) initial charges, where the position of the ions was compiled into a histogram as a function of the trap radius and illustrated for selected time intervals of the simulation, e.g., from 0 to 2 μs. The data were normalized with the radial volume and mirrored for illustration only with respect to the zero-radius.

The dashed line demonstrates the initial ion distribution at time zero. In the case of (a), the radial distribution slowly expands to an average radius of about 2.5 mm and no change in the distribution is observed after 10 μs. No ions are lost in this process, as the ion distribution does not approach the trap rods at a radius of 4.5 mm. By contrast, for initially 10^9e in (b), the expansion occurs more rapidly and ions are lost when exceeding 4.5 mm (these ions are no longer considered for the space-charge). Due to this loss in charges, the average ion radius reduces again. At this time, about 66% of the ions are still left in the trap (8-10 μs), and for later times, the distribution remains stable with an average radius of about 3 mm. This indicates that the equilibrium condition is obtained at a total number of charges of $\sim 6 \times 10^8 e$.

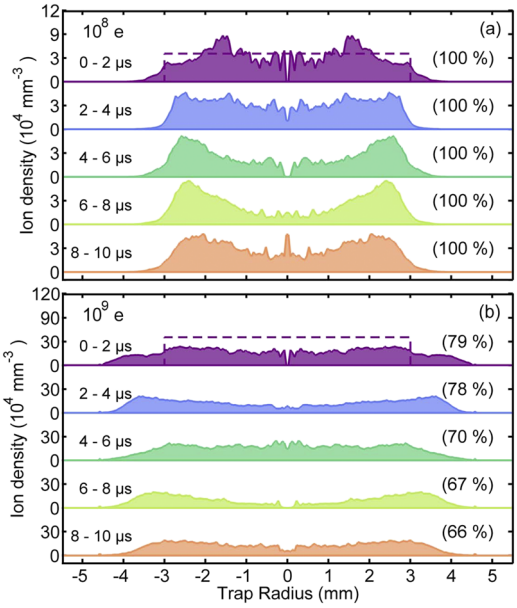

FIG. 9. Simulation of the space-charge limited ion capacity of the present ion trap: Ions are simulated in an octupole field with trapping potential from Fig. 5. The initial total number of charges was 10^8e in (a) and 10^9e in (b). The location of the ions in the radial direction is averaged over different times of the simulation (e.g., 0 to 2 μs). The dashed line demonstrates the initial ion distribution at time zero. The data were mirrored for illustration only and normalized with the radial volume. The trap rods are located at −4.5 mm and +4.5 mm.

Thus, we estimate the maximum number of ions that can be trapped at about 6×10^8 ions. Majima *et al.*[33] found a limit of 1.2×10^9 ions for the same RF amplitude but 3 MHz instead of 1.2 MHz and with a four times longer trap and slightly larger trap radius.

C. Simulations of the acceleration tube

The 200 mm long acceleration tube serves as a shielded environment for the ion bunch and is quickly switched between a low negative voltage (≥−300 V) to a positive high-voltage of up to +20 kV (operation for positive ions). The negative voltage is used for the ion injection and is matched to the DC voltage of the last octupole OG8. Even lower negative voltages can be applied to slightly accelerate the ions into the tube and improve the transfer efficiency from the octupole. However, higher initial kinetic energy shortens the tube time-of-flight and increases the ion bunch length.

The design of the acceleration tube, the simulated trajectories, and the potential in longitudinal direction for ions entering and leaving the tube are shown in Fig. 10. Positive ions were created randomly with a kinetic energy of 20 eV in octupole guide OG8, which is kept at −20 V. The ions enter the tube at a potential of −300 V, which is switched to +9700 V to obtain ions with a kinetic energy of 10 keV. A conical acceleration lens focuses the beam after acceleration and uses the same voltage as the tube. Finally, an einzel lens is used to change the focusing of the ion beam, which is confirmed by measuring the beam size on the MCP detector. For the ion transport to the RICE, a quadrupole doublet is utilized to further manipulate the beam (see Fig. 1).

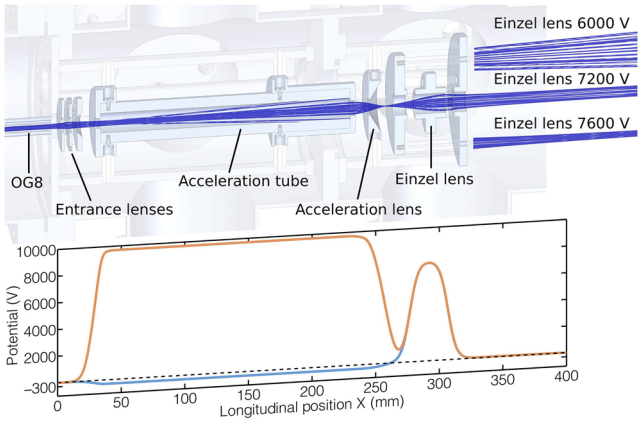

FIG. 10. Side view of the acceleration tube (AT): simulated ion trajectory (blue) starting from the last octupole guide OG8. Different beam focusing by einzel lens voltage. The electrostatic potential along the longitudinal direction is shown for the ion injection (blue: AT at −300 V) and acceleration (orange: AT at +9700 V) to create ions with a kinetic energy of 10 keV. The black dashed line marks the ground potential (0 V).

The dimension of the tube was chosen to match the RICE revolution time, which depends on the ring circumference (~3 m), and the ion's mass and kinetic energy (up to 20 keV). Typically, the ions from OG8 have about 20 eV and are further accelerated into the tube to about 100 eV. Thus, the energy ratio between ions entering and leaving the acceleration tube is about 200 and the length ratio between the ring and the tube should be chosen as 3 m/$\sqrt{200} \approx 200$ mm.

IV. CHARACTERIZATION MEASUREMENTS

A. Electrospray ionization source

For the characterization measurements, the home-built ESI source has been employed, which was already described beforehand (Fig. 2). Although experiments with different ion species were performed, methylene blue cations MB^+ were used for all the following measurements (due to experiences in our collaboration[23]). This organic chloride salt is also known as methylthioninium chloride ($C_{16}H_{18}ClN_3S$) and decomposes in aqueous solution to $C_{16}H_{18}N_3S^+$ and chloride anion Cl^-. For the ESI solution, we used a 7:3 mixture of acetonitrile (CH_3CN) with water and added 5×10^{-4} mol/l of methylene blue. With a moderately heavy ion mass of 284 amu, it is well suited for the characterization of the ion beamline.

Figure 11 shows a mass spectrum using the quadrupole mass filter and measuring the ion count rate on the CEM detector downstream of the trap. Multiple water clusters attached to methylene blue are observed [$MB^+(H_2O)_n, n \leq 60$]. By heating the ESI capillary into the vacuum system to 54 °C, the water clusters can be largely reduced. Minor contributions from dissociation can also be observed for masses smaller than the MB^+ peak.

For even higher capillary temperatures, methylene blue is the dominant ion species. Thus, to avoid loosing ions to a large extent due to the low quadrupole mass filter transmission (~20%), the mass-selection capability of the quadrupole is sometimes not used assuming MB^+ is dominant.

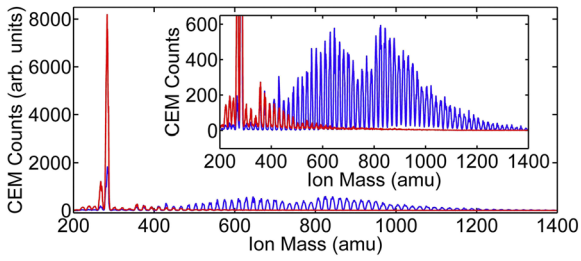

FIG. 11. Mass spectrum of methylene blue water clusters using the quadrupole mass: capillary temperatures of 20 °C (blue) and 54 °C (red) were used, respectively.

B. Cryogenic ion trap

In this section, we report on ion measurements performed with the CEM detector in pulse counting mode using methylene blue cations from the ESI source. As the essential results of these trap studies can be acquired at room temperature, the following measurements did not take advantage of the cryogenic design of the trap. The ions were injected as a continuous beam into the trap, while helium was introduced in a pulsed mode with a rate of 10 Hz. The backing pressure of the helium was optimized with a needle valve before the pulsed valve to achieve the highest ion yield after trap extraction. As already explained in the section about the vacuum system, this resulted in an averaged vacuum pressure of about $\sim 10^{-2}$ Pa measured about half a meter below the trap. The pressure in the trap from one helium pulse was found to recover within ~100 ms, after which ions can again pass through the trap without experiencing collisions. This was determined from the time-dependent count rate of a continuous beam of ions on the CEM after a helium pulse was injected. Hence, no helium is injected before and during the ion extraction to prevent their reheating by heavy ion-helium collisions. During a short trapping time in the order of micro- to milliseconds, both trap end-caps (EC1/EC2) are at a high potential (usually +100 V). Afterwards, the ions are extracted by switching the fin-voltages and simultaneously lowering the voltage on the exit end-cap EC2 (see Fig. 5).

An example of this measurement is shown in Fig. 12 for different fin-voltages in comparison. The case (a) shows ion injection durations of 100 ms; here, only one helium pulse was

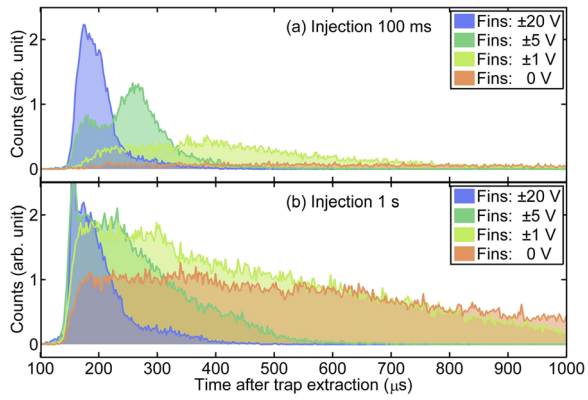

FIG. 12. Extracted ion bunch of MB^+ from the trap measured at the CEM detector for different fin voltages of ±20 V, ±5 V, ±1 V, and 0 V with a trap ion injection duration of 100 ms (a) and 1 s (b).

injected at the beginning of the ion injection. With increasing fin-voltages, the focusing of the ion bunch is improved and the time of flight to the CEM detector decreases. With fin-voltages of ±20 V (and $V_{OG6} = V_{OG7} = -20$ V), a bunch length (FWHM) of ~55 μs is achieved.

Comparison of these bunch shapes to the simulations (Fig. 8) clearly shows a similarity to the case of low kinetic energy of the ions with 0.05 eV or 0.1 eV [Figs. 8(b) and 8(c)]. A similar well-defined bunch shape as in the simulation is observed in Fig. 12(a) for fin-voltages of ±20 V as well as the double-peak structure for ±5 V and a shallow longer bunch in the case of ±1 V. From these indications in the time-of-flight distribution, we would expect a kinetic energy of the trapped ions below 0.1 eV. This is consistent with ions at room temperature and a more precise analysis cannot be expected, as the bunch shapes in Fig. 8 for 0.1 eV and below are too similar.

By contrast, the measurements in Fig. 12(b) with an ion injection duration of 1 s cannot be well compared to the simulations as the high space-charge effect during the ion extraction influences the time of flight. It is noted that due to the saturation of the detector, high ion count rates above the value of 2 in Fig. 12 are not reliable. This value corresponds to high count rates above 10^6 cps, where individual ion counts on the CEM cannot be well distinguished.

Due to this reason as well as uncalibrated signal amplification factors, the absolute number of ions cannot be determined with this method. To obtain information on the ion number in the bunch, we directly collect the charge of the ions on the rods of the octupole guide OG7, by assuming that secondary electron emission is negligible at these low ion energies. Without the applied RF, the ions will spread out in the ion guide and impinge on the rods. We utilized a fast current preamplifier (ITHACO model 1211) to convert the charge to a voltage signal and applied a small negative bias voltage (typically −18 V) to the rods to improve the ion collection.

Figure 13 summarizes the obtained number of ions (number of charges) collected on the octupole OG7, which were extracted from the trap after loading for different injection durations. For consistency, all measurements were taken with fin-voltages of ±20 V. The signal for mass-selected methylene blue cations MB^+ collected on OG7 shows a linear increase in the number of ions as a function of the injection duration up to 10 s (blue squares). Thus, even for these long injection durations, ions can be efficiently and continuously injected, and the trap cycle works as expected. For an injection time of 10 s, about 6×10^7 ions were trapped and extracted.

For higher ion intensity, when the mass-selection capability of the quadrupole mass filter is not utilized (specified transmission of 20% for mass-filtering), this tendency is found to be not linear anymore beyond 1 s of injection duration. The obtained plateau at about 1.2×10^8 ions (Fig. 13, green circles) suggests that the space-charge limit of the trap is reached. This value is in the same order of magnitude as the simulated value of 6×10^8 ions. The discrepancy could be due to the loss of ions during the trap extraction, which cannot be measured on OG7 or an overestimation of the space-charge due to the crude approximation with multiple charges in the simulation. Considering these aspects, the experimentally determined value of 1.2×10^8 ions represents a minimum value for the space-charge limit and thus is in reasonable agreement with the simulation.

C. Pulsed high-voltage acceleration

The pulsed high-voltage acceleration tube is used to bring the bunched ions to 10-20 keV kinetic energies. The ion detection is realized with the MCP detector, which is about 0.7 m downstream of the acceleration. The MB^+ ions are again extracted from the trap with fin voltages of ±20 V and $V_{OG6} = V_{OG7} = V_{OG8} = -20$ V. The ion bunch shape was at first determined with the CEM detector (Fig. 14, gray area). It is noted that a 20 eV MB^+ beam has a time-of-flight (TOF) through the acceleration tube of about 54 μs, and hence the CEM bunch in Fig. 14 fits completely into the tube and can be accelerated.

However, to improve the tube transmission, the ion bunch was here additionally accelerated into the tube with a negative voltage of −300 V. The ion's TOF through the tube is then only ~14 μs and the MB^+ bunch will be truncated, when the high-voltage is switched on. Figure 14 illustrates the result under this condition, showing the ion counts from the MCP as a function of the time after trap extraction (blue). The entire bunch, however, can be reconstructed by varying the time delay between the bunch arrival at the acceleration tube and the switching of the high-voltage (here +10 kV). To perform this measurement,

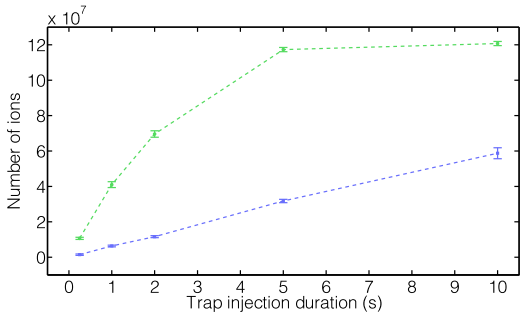

FIG. 13. Determined number of ions measured on octupole OG7 after ion trap extraction as a function of the trap injection duration. Low ion intensity using mass-selected methylene blue cation MB^+ (blue squares) and high ion intensity without mass-filtering (green circles). The error bars are only from the statistical deviation of 20 individual measurements for each setting. Dashed lines are to guide the eye.

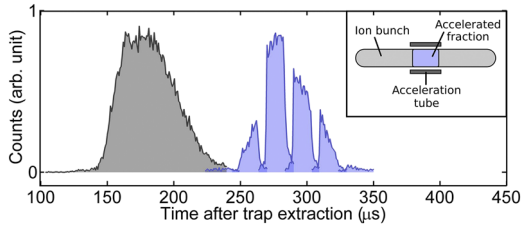

FIG. 14. MCP detector count rate as a function of time after trap extraction: The MB^+ ion bunch detected with the CEM is shown in gray. Measurements of the counts on the MCP detector with different tube switching delay times are shown in blue using a reduced ion intensity to avoid saturation of the detector. In this example, the bunch was accelerated by −300 V into the acceleration tube to improve the transmission prior to high-voltage acceleration to 10 keV. Due to this, only a part of the ion bunch is accelerated at a time, but the entire bunch shape could be reconstructed by changing the tube switching delay.

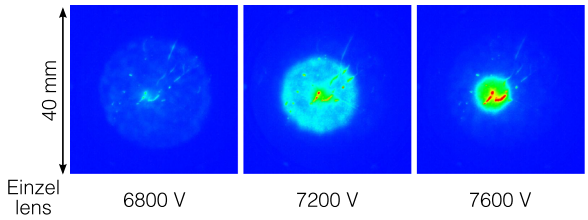

FIG. 15. Camera images from the phosphor screen behind the MCP detector (40 mm diameter) of single accelerated MB^+ ion bunches. The einzel lens voltage was varied to manipulate the ion's focusing.

the ion intensity from the ESI to the trap was greatly decreased, and a reduced count rate is observed on the MCP so that all parts of the truncated ion bunch are found to be below the saturation limit of the detector.

A good agreement is observed between the bunch shape measured on the CEM and the reconstructed bunch on the MCP, although the bunches are not expected to be exactly the same, as the drift from the CEM to the acceleration tube as well as the acceleration with −300 V will change the bunch shape.

The transversal size of the beam was also measured using a phosphor screen behind the MCP and a digital camera which was synchronized with the pulsed high-voltage of the tube. Depending on the einzel lens voltage, the beam size changed as expected (Fig. 15) and good agreement was found with the simulations of defocused, parallel, and focused beams (Fig. 10). It is noted that the beam can be further manipulated by using the quadrupole doublet (see Fig. 1) behind the acceleration tube to optimize the transport to the RICE injection beamline.

V. CONCLUSION AND OUTLOOK

In this work, we have presented an ion preparation beamline for accumulation, cooling, and acceleration of ion bunches for the injection into the cryogenic storage ring RICE. Molecular ions are produced in an ESI source at low velocity, mass-selected, and injected as a continuous ion beam into the cryogenic octupole ion trap. The new concept of fast ion extraction from an octupole ion trap, using two sets of wedge-shaped electrodes (Fins) between the trap rods, was successfully studied. For our test molecular ion MB^+, a good condition for the extraction was found with a combination of fin-voltages at ±20 V and octupole DC voltages of −20 V for OG6/7/8; for ions with different masses, these values need to be adjusted. The length of the measured ion bunch of the trap-extracted ions was in the order of 50 μs and is well suited to create keV ion bunches in the pulsed ion acceleration tube.

The understanding of this system further benefited from ion trajectory simulations which could be well compared to the experimental observations. Excellent agreement was here observed between the simulated and measured ion bunch shapes at the location of the CEM detector. For high ion intensities in the trap (≥1 s injection duration), influences from Coulomb repulsion were found in these bunch shapes and discrepancies to the simulation, which neglected these effects. We thus further investigated the space-charge limit of the present trap through experiments and simulations. The total number of ions that can be trapped was experimentally estimated to be $\sim 1.2 \times 10^8$ by measuring the number of extracted charges. A crude simulation of ions in an octupole trap with Coulomb repulsion was found to be sufficient to confirm this experimental observation with a simulated value of $\sim 6 \times 10^8$.

Current investigations are intended to optimize the ion injection of the keV ion bunches into RICE. Although the presented measurements were taken at room temperature, trap operation and high-voltage acceleration have also been tested for cryogenic trap temperatures. The effect of the cryogenic cooling of the ions on their internal degrees of freedom will be tested in future spectroscopic measurements in RICE.

ACKNOWLEDGMENTS

This work was supported by the RIKEN Basic Science Interdisciplinary Research Projects, the RIKEN Pioneering Projects, and JSPS KAKENHI Grant No. 26220607. Y.N. acknowledges the financial support from JSPS KAKENHI Grant Numbers 16K13859, 17H02993, 18K18790. Y.E. is supported by the Special Postdoctoral Researchers Program of RIKEN. T.M. acknowledges the financial support from Matsuo Foundation. Initial developments on the ESI from K. Ohshimo and fruitful discussions with T. Furukawa are gratefully acknowledged.

[1] D. Gerlich, in *State-Selected State-to-State Ion-Molecule Reaction Dynamics Advances in Chemical Physics, Part 1. Experiment*, Advances in Chemical Physics, edited by C.-Y. Ng and M. Baer (John Wiley & Sons, Inc., New York, 1992), Vol. 82, pp. 1–176.
[2] O. V. Boyarkin, S. R. Mercier, A. Kamariotis, and T. R. Rizzo, J. Am. Chem. Soc. **128**, 2816 (2006).
[3] A. B. Wolk, C. M. Leavitt, E. Garand, and M. A. Johnson, Acc. Chem. Res. **47**, 202 (2014).
[4] H. Yao and R. A. Jockusch, J. Phys. Chem. A **117**, 1351 (2013).
[5] M. H. Stockett, J. Houmøller, K. Støchkel, A. Svendsen, and S. Brøndsted Nielsen, Rev. Sci. Instrum. **87**, 053103 (2016).
[6] S. P. Møller, Nucl. Instrum. Methods Phys. Res., Sect. A **394**, 281 (1997).
[7] T. Tanabe, K. Chida, K. Noda, and I. Watanabe, Nucl. Instrum. Methods Phys. Res., Sect. A **482**, 595 (2002).
[8] S. Jinno, T. Takao, Y. Omata, A. Satou, H. Tanuma, T. Azuma, H. Shiromaru, K. Okuno, N. Kobayashi, and I. Watanabe, Nucl. Instrum. Methods Phys. Res., Sect. A **532**, 477 (2004).
[9] D. Zajfman, O. Heber, L. Vejby-Christensen, I. Ben-Itzhak, M. Rappaport, R. Fishman, and M. Dahan, Phys. Rev. A **55**, R1577 (1997).
[10] H. T. Schmidt, R. D. Thomas, M. Gatchell, S. Rosén, P. Reinhed, P. Löfgren, L. Brännholm, M. Blom, M. Björkhage, E. Bäckström, J. D. Alexander, S. Leontein, D. Hanstorp, H. Zettergren, L. Liljeby, A. Källberg, A. Simonsson, F. Hellberg, S. Mannervik, M. Larsson, W. D. Geppert, K. G. Rensfelt, H. Danared, A. Paál, M. Masuda, P. Halldén, G. Andler, M. H. Stockett, T. Chen, G. Källersjö, J. Weimer, K. Hansen, H. Hartman, and H. Cederquist, Rev. Sci. Instrum. **84**, 055115 (2013).
[11] R. von Hahn, A. Becker, F. Berg, K. Blaum, C. Breitenfeldt, H. Fadil, F. Fellenberger, M. Froese, S. George, J. Göck, M. Grieser, F. Grussie, E. A. Guerin, O. Heber, P. Herwig, J. Karthein, C. Krantz, H. Kreckel, M. Lange, F. Laux, S. Lohmann, S. Menk, C. Meyer, P. M. Mishra, O. Novotný, A. P. O'Connor, D. A. Orlov, M. L. Rappaport, R. Repnow, S. Saurabh, S. Schippers, C. D. Schröter, D. Schwalm, L. Schweikhard, T. Sieber, A. Shornikov, K. Spruck, S. Sunil Kumar, J. Ullrich, X. Urbain, S. Vogel, P. Wilhelm, A. Wolf, and D. Zajfman, Rev. Sci. Instrum. **87**, 063115 (2016).
[12] Y. Nakano, Y. Enomoto, T. Masunaga, S. Menk, P. Bertier, and T. Azuma, Rev. Sci. Instrum. **88**, 033110 (2017).
[13] M. Lange, M. Froese, S. Menk, J. Varju, R. Bastert, K. Blaum, J. R. C. López-Urrutia, F. Fellenberger, M. Grieser, R. von Hahn, O. Heber, K.-U. Kühnel, F. Laux, D. A. Orlov, M. L. Rappaport, R. Repnow, C. D. Schröter, D. Schwalm, A. Shornikov, T. Sieber, Y. Toker, J. Ullrich, A. Wolf, and D. Zajfman, Rev. Sci. Instrum. **81**, 055105 (2010).

[14]C. J. Johnson, B. B. Shen, B. L. J. Poad, and R. E. Continetti, Rev. Sci. Instrum. **82**, 105105 (2011).
[15]Z. Amitay, D. Zajfman, and P. Forck, Phys. Rev. A **50**, 2304 (1994).
[16]C. Meyer, A. Becker, K. Blaum, C. Breitenfeldt, S. George, J. Göck, M. Grieser, F. Grussie, E. A. Guerin, R. von Hahn, P. Herwig, C. Krantz, H. Kreckel, J. Lion, S. Lohmann, P. M. Mishra, O. Novotný, A. P. O'Connor, R. Repnow, S. Saurabh, D. Schwalm, L. Schweikhard, K. Spruck, S. Sunil Kumar, S. Vogel, and A. Wolf, Phys. Rev. Lett. **119**, 023202 (2017).
[17]H. T. Schmidt, G. Eklund, K. C. Chartkunchand, E. K. Anderson, M. Kamińska, N. de Ruette, R. D. Thomas, M. K. Kristiansson, M. Gatchell, P. Reinhed, S. Rosén, A. Simonsson, A. Källberg, P. Löfgren, S. Mannervik, H. Zettergren, and H. Cederquist, Phys. Rev. Lett. **121**, 079901 (2018).
[18]H. T. Schmidt, G. Eklund, K. C. Chartkunchand, E. K. Anderson, M. Kamińska, N. de Ruette, R. D. Thomas, M. K. Kristiansson, M. Gatchell, P. Reinhed, S. Rosén, A. Simonsson, A. Källberg, P. Löfgren, S. Mannervik, H. Zettergren, and H. Cederquist, Phys. Rev. Lett. **119**, 073001 (2017).
[19]N. de Ruette, M. Wolf, L. Giacomozzi, J. D. Alexander, M. Gatchell, M. H. Stockett, N. Haag, H. Zettergren, H. T. Schmidt, and H. Cederquist, Rev. Sci. Instrum. **89**, 075102 (2018).
[20]M. Yamashita and J. B. Fenn, J. Phys. Chem. **88**, 4451 (1984).
[21]J. Fenn, M. Mann, C. Meng, S. Wong, and C. Whitehouse, Science **246**, 64 (1989).
[22]A. C. Leney and A. J. R. Heck, J. Am. Soc. Mass Spectrom. **28**, 5 (2017).
[23]T. Sato, T. Majima, K. Hashimoto, K. Hashimoto, Y. Zama, J. Matsumoto, H. Shiromaru, K. Okuno, H. Tanuma, and T. Azuma, Eur. Phys. J. D **63**, 189 (2011).
[24]R. M. Jones and S. L. Anderson, Rev. Sci. Instrum. **71**, 4335 (2000).
[25]F. Herfurth, J. Dilling, A. Kellerbauer, G. Bollen, S. Henry, H. J. J. J. Kluge, E. Lamour, D. Lunney, R. B. Moore, C. Scheidenberger, S. Schwarz, G. Sikler, and J. Szerypo, Nucl. Instrum. Methods Phys. Res., Sect. A **469**, 254 (2001).
[26]J. Mikosch, U. Frühling, S. Trippel, R. Otto, P. Hlavenka, D. Schwalm, M. Weidemüller, and R. Wester, Phys. Rev. A **78**, 023402 (2008).
[27]A. Loboda, A. Krutchinsky, O. Loboda, J. McNabb, V. Spicer, W. Ens, and K. Standing, Eur. J. Mass Spectrom. **6**, 531 (2000).
[28]F. Martinez, S. Bandelow, C. Breitenfeldt, G. Marx, L. Schweikhard, A. Vass, and F. Wienholtz, Int. J. Mass Spectrom. **365-366**, 266 (2014).
[29]B. E. Wilcox, C. L. Hendrickson, and A. G. Marshall, J. Am. Soc. Mass Spectrom. **13**, 1304 (2002).
[30]W. C. Wiley and I. H. McLaren, Rev. Sci. Instrum. **26**, 1150 (1955).
[31]D. A. Dahl, Int. J. Mass Spectrom. **200**, 3 (2000).
[32]MATLAB, The MathWorks, Inc., Natick, Massachusetts, United States.
[33]T. Majima, G. Santambrogio, C. Bartels, A. Terasaki, T. Kondow, J. Meinen, and T. Leisner, Phys. Rev. A **85**, 053414 (2012).